Received: 22 July 2021 | Revised: 29 September 2021 | Accepted: 30 September 2021

DOI: 10.1002/col.22747

RESEARCH ARTICLE

COLOR RESEARCH AND APPLICATION WILEY

Appearance synthesis of fluorescent objects with mutual illumination effects

Shoji Tominaga[1,2] | **Giuseppe Claudio Guarnera**[1,3]

[1]Department of Computer Science, Norwegian University of Science and Technology, Gjøvik, Norway

[2]Department of Business and Informatics, Nagano University, Ueda, Japan

[3]Department of Computer Science, University of York, York, UK

Correspondence
Shoji Tominaga, Department of Computer Science, Norwegian University of Science and Technology, Gjøvik, Norway; Nagano University, Ueda, Japan.
Email: shojitominaga12@gmail.com

Funding information
the Research Council of Norway, Grant/Award Number: N-288670; Japan Society for the Promotion of Science, Grant/Award Number: JP20K11893

Abstract

We propose an approach for the appearance synthesis of objects with matte surfaces made of arbitrary fluorescent materials, accounting for mutual illumination. We solve the problem of rendering realistic scene appearances of objects placed close to each other under different conditions of uniform illumination, viewing direction, and shape, relying on standard physically based rendering and knowledge of the three-dimensional shape and bispectral data of scene objects. The appearance synthesis model suggests that the overall appearance is decomposed into five components, each of which is expanded into a multiplication of spectral functions and shading terms. We show that only two shading terms are required, related to (a) diffuse reflection by direct illumination and (b) interreflection between two matte surfaces. The Mitsuba renderer is used to estimate the reflection components based on the underlying Monte Carlo simulation. The spectral computation of the fluorescent component is performed over a broad wavelength range, including ultraviolet and visible wavelengths. We also address a method for compensating for the difference between the simulated and real images. Experiments were performed to demonstrate the effectiveness of the proposed appearance synthesis approach. The accuracy of the proposed approach was experimentally confirmed using objects with different shapes and fluorescence in the presence of complex mutual illumination effects.

KEYWORDS

appearance synthesis, fluorescence, mutual illumination, physically based rendering

1 | INTRODUCTION

1.1 | Background

Fluorescence is an optical phenomenon in which a material is first excited by light radiation in a specific wavelength region; when the excited state relaxes, it emits light radiation at a longer wavelength.[1,2] Fluorescence substances with such characteristics are often incorporated into objects made of materials such as paper, paint, plastic, dye, and cloth to improve the visual appearance in comparison to the surface of a nonfluorescent reflective object. In fact, when a fluorescent substance is applied, the surfaces of most fluorescent objects appear brighter and more vivid compared with the original color surface because of the self-luminescence through the fluorescent emission.

Fluorescent spectral characteristics are described in terms of the bispectral radiance factor, which is a function of two variables: the excitation wavelength of the incident light, and the emission/reflection wavelength. The bispectral radiance factor can be summarized by the Donaldson matrix[3,4] (also known as the re-radiation matrix[5]), which is an illuminant-independent matrix representation of the bispectral characteristics of a material. Knowledge of the Donaldson matrix allows spectral rendering of the color appearance of an object under any arbitrary light source with a known spectral power distribution.

The overall appearance of three-dimensional (3D) objects in a scene results from a combination of chromatic factors (such as spectral reflectance, luminescence spectra, and scene illuminant) and shading terms (object geometry, texture, position, and shape of the light source). In addition, real scenes often exhibit significant mutual illumination (or interreflection) between surfaces.[6,7] Because mutual illumination affects the surface appearance, its influence must be accounted for.[8,9] Clearly, the effect of mutual illumination depends on both the surface materials and the geometries. With the growing importance of fluorescent materials, comprehensive approaches to rendering fluorescent objects while accounting for mutual illumination effects have received much attention. Tominaga et al[10,11] proposed an image-based approach for the appearance reconstruction of flat fluorescent objects with mutual illumination effects. This approach requires multiple images of the same object under different illumination directions. It is limited to planar fluorescent surfaces, as a generalization to more complex and realistic cases, such as curved fluorescent surfaces, is challenging to achieve without using 3D shape data. Jung et al[12] proposed a bidirectional rendering method for fluorescence, where different strategies were discussed for mollifying δ-component (reflectance component) in Donaldson matrices. Mollifiers are sequences of smooth functions approximating nonsmooth functions. In the context of light transport, the integration might contain Dirac delta functions, for instance when mirror-like objects are present in the scene. In Reference 12, the delta functions are replaced by a sequence of functions that converges to the delta function itself. Such a sequence, the *mollifier*, has a smoothening effect on the singularities introduced by the delta functions. However, the spectral mollification strategy produces a color bias for object surfaces with normal reflectance under a continuous illuminant spectrum.

1.2 | Proposed approach

In this article, we propose a novel approach to the appearance rendering of fluorescent objects with mutual illumination effects. Our method relies on physically based simulation, where the interaction between light and object materials is precisely simulated using an off-the-shelf renderer. As such, it does not require the acquisition of multiple images of the same object, but only knowledge of the 3D shape of the objects. The spectral model for mutual illumination is based on one bounce (path length 2) between two objects, whereas no approximation is applied to the bispectral functions in the Donaldson matrices. Figure 1 shows one of the objects used in this study, where the figure is reproduced in the RGB color mode converted from the spectral data. The ground truth image of the target scene was captured using a spectral imaging system under an artificial sunlight source. The target object consists of two halves of a cylinder composed of two different fluorescent sheets (yellow and red). The two half cylinders are in contact with the strong mutual illumination at the concave connection areas of the two cylinders.

In Section 2, we describe the foundation of the spectral appearance model of fluorescent objects. When two matte surfaces of fluorescent objects are close to each other, the spectral image formation model can be described by their spectral reflectance, excitation, emission, and illuminant spectrum. Mutual illumination is modeled spectrally by a single bounce of indirect illumination between two surfaces. We show that the appearance can be decomposed into five components, which can be further expanded into a multiplication of spectral functions and shading terms, where the spectral functions are inherent to each fluorescent material and illuminant, while the shading terms change according to the object's shape and viewpoint/light source position.

In Section 3, we develop an appearance synthesis method based on a physically-based simulation. Our spectral computation is performed over a broad wavelength range, including ultraviolet (UV) and visible wavelengths. The image is constructed using a linear

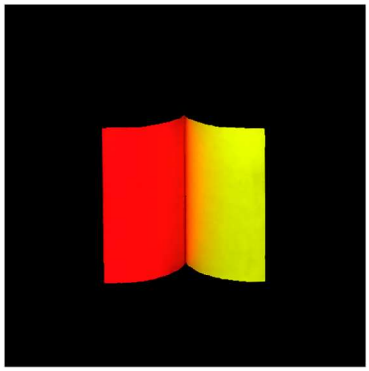

FIGURE 1 Acquired color image of two fluorescent half cylinders

combination of the five components of the overall appearance. Building upon the similarity between diffuse reflection and fluorescent emission, the shading for mutual illumination can be further simplified to the reflection component only. The Mitsuba renderer is used to estimate the reflection components based on the underlying Monte Carlo spectral simulation. We show that the simulated interreflection component is often underestimated with respect to a real scene. Therefore, we devise an approach to compensate for the difference between the rendered and the real images.

In Section 4, we present experimental results and demonstrate the effectiveness of the proposed appearance synthesis approach. The rendered images for fluorescent objects with different shapes and complex mutual illumination effects, are compared with the ground truth images acquired using a spectral imaging system. The accuracy is also assessed using performance indices.

2 | DATA ACQUISITION AND APPEARANCE MODELING

2.1 | Equipment and data acquisition

The spectral imaging system used for spectral image acquisition consisted of a monochrome CCD camera with Peltier cooling, 12-bit dynamic range, 1280-by-1024 pixel resolution, a VariSpec liquid crystal tunable filter, an IR cut filter, and a personal computer (see[13]). The spectral images of fluorescent objects were captured at 5 nm intervals in the visible wavelength range (400-700 nm); thus, each captured image was represented in an array of 61-dimensional vectors. For the light source, we used an artificial sunlight lamp (SERIC, SOLAX 100 W). The spectral power distribution, uniformly sampled by 71 points in the 350 to 700 nm range, is shown in Figure 2. A 3D scanner GOM ATOS TripleScan was used to measure the 3D shape of objects. The number of points acquired for each object in the scene was in the range of 10 000 to 30 000 points.

2.2 | Bispectral model of a fluorescent object

The fluorescent characteristics are well described in terms of the bispectral radiance factor, which is a function of two wavelength variables: the excitation wavelength of the incident light, and the emission and reflection wavelength of the output light. The Donaldson matrix is a discrete representation of the bispectral radiance factor. This matrix can be directly measured using

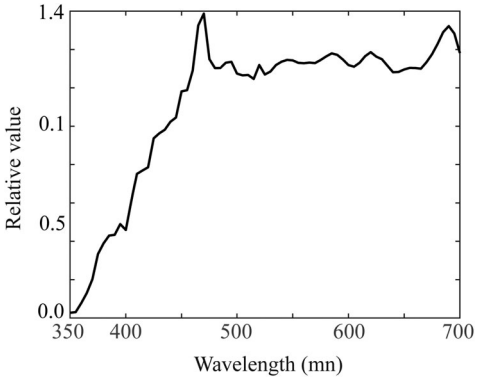

FIGURE 2 Spectral-power distribution of the artificial sunlight lamp

two monochromators[14] or one monochromator with short-wavelength cutoff filters.[15,16] However, these measurement methods were inconvenient and impractical in ordinary scenes using an imaging system. Several approaches have been proposed for estimating the Donaldson matrix using various types of imaging systems, such as RGB cameras,[17] multiband imaging systems,[18,19] and spectral imaging systems.[4,13]

Let us represent the Donaldson matrix as a two-variable function $D(\lambda_{em},\lambda_{ex})$ of the excitation wavelength λ_{ex} and the emission/reflection wavelength λ_{em}. The excitation wavelength for many fluorescent materials starts from approximately 330 to 350 nm (see[16]). Because most light sources used in everyday life contain some UV components that contribute to fluorescent emission, the excitation range is set at $350 \le \lambda_{ex} \le 700$ nm in this study, which includes UV and visible wavelengths. On the other hand, because common imaging systems operate in the visible wavelength range for the human visual system, the emission/reflection range is set to $400 \le \lambda_{em} \le 700$ nm. The Donaldson matrix is decomposed into two components: the reflected radiance factor $D_R(\lambda_{em},\lambda_{ex})$ associated with light reflection, and the luminescent radiance factor $D_L(\lambda_{em},\lambda_{ex})$ associated with fluorescent emission. The matrix $D_R(\lambda_{em},\lambda_{ex})$ is diagonal and has values $\lambda_{em} = \lambda_{ex}$ corresponding to the surface spectral reflectance $S(\lambda)$. The matrix $D_L(\lambda_{em},\lambda_{ex})$ contains values in the off-diagonal $\lambda_{em} > \lambda_{ex}$ because of the Stokes shift (see Reference 2). Typically, a fluorescent object contains a single fluorescent chemical compound. Under this assumption, the luminescent radiance factor is separated into a multiplication of the emission and excitation spectra $D_L(\lambda_{em},\lambda_{ex}) = \alpha(\lambda_{em})\beta(\lambda_{ex})$ (see Reference 4). This multiplication suggests that one of the two spectra $\alpha(\lambda_{em})$ and $\beta(\lambda_{ex})$ can be arbitrarily rescaled. Therefore, we assume that the excitation spectrum is normalized to $\int_{350}^{700}\beta(\lambda_{ex})d\lambda_{ex} = 1$.

A discrete form of the Donaldson matrix with the above properties can be represented as

$$\mathbf{D} = \mathbf{D}_{\mathrm{R}} + \mathbf{D}_{\mathrm{L}} = \begin{bmatrix} \alpha_1\beta_1 & \cdots & \alpha_1\beta_{m-n} & s_1 & 0 & \cdots & 0 \\ \alpha_2\beta_1 & & \alpha_2\beta_{m-n} & \alpha_2\beta_{m-n+1} & s_2 & \ddots & \vdots \\ \vdots & & \vdots & \vdots & \ddots & \ddots & 0 \\ \alpha_n\beta_1 & \cdots & \alpha_n\beta_{m-n} & \alpha_N\beta_{m-n+1} & \cdots & \alpha_n\beta_{m-1} & s_n \end{bmatrix}, \quad (1)$$

where s_i ($i = 1, 2, ..., n$), α_i ($i = 1, 2, ..., n$), and β_i ($i = 1, 2, ..., m-1$) represent the discrete spectral representations of the reflectance, emission, and excitation, respectively. In the present study, we sample the spectral functions at equal wavelength intervals of 5 nm; thus, the Donaldson matrix is described by $m = 71$ and $n = 61$.

Figure 3A shows the Donaldson matrix of the red object in Figure 1, whereas Figure 3B shows the yellow object. Humps in the emission wavelength ranges of 600 to 700 nm and 500 to 600 nm represent the luminescent radiation factors of orange and green colors, respectively.

2.3 | Image formation model of objects with mutual illumination

Mutual illumination is observed when multiple objects are located close to each other: light reflected from a surface, directly illuminated by a light source, bounces onto a second surface, then possibly back to the first surface, and so on until it reaches the sensor. The associated intensity decreases rapidly with each bounce. The first bounce between the two surfaces constitutes the most significant contribution to the interreflection and could suffice for modeling it (see Reference 6). Deeb et al[7] proposed a spectral infinite-bounce model between two flat matte surfaces of nonfluorescent objects. For fluorescent objects, Tominaga et al[8] analyzed spectral images including mutual illumination effects observed between two matte fluorescent surfaces, and showed that the spectral composition could be described with four spectral components. The analysis results are summarized in the following.

The spectral radiance at position $\mathbf{x} = (x, y, z)$ on the surface of a matte object made of fluorescent material, observed under a single illuminant $E(\lambda)$, can be described as a continuous function of wavelength

$$y(\mathbf{x}, \lambda_{\mathrm{em}}) = f_{\mathrm{ref}}(\mathbf{x}) S(\lambda_{\mathrm{em}}) E(\lambda_{\mathrm{em}}) + f_{\mathrm{lum}}(\mathbf{x}) \alpha(\lambda_{\mathrm{em}}) \int_{350}^{\lambda_{\mathrm{em}}} \beta(\lambda_{\mathrm{ex}}) E(\lambda_{\mathrm{ex}}) d\lambda_{\mathrm{ex}}, \quad (2)$$

where the first and second terms on the right-hand side of the equation represent the reflection radiance and luminescence radiance, respectively. We refer to the weights $f_{\mathrm{ref}}(\mathbf{x})$ and $f_{\mathrm{lum}}(\mathbf{x})$ for the spectral functions as *shading terms*, which depend on the object surface geometry and position.

There are previous considerations regarding the directional properties of fluorescent emission.[20-23] Treibitz et al[21] suggested that when a fluorescent object is illuminated, it re-emits light isotropically, similar to a Lambertian surface reflecting light. Tominaga et al[22]

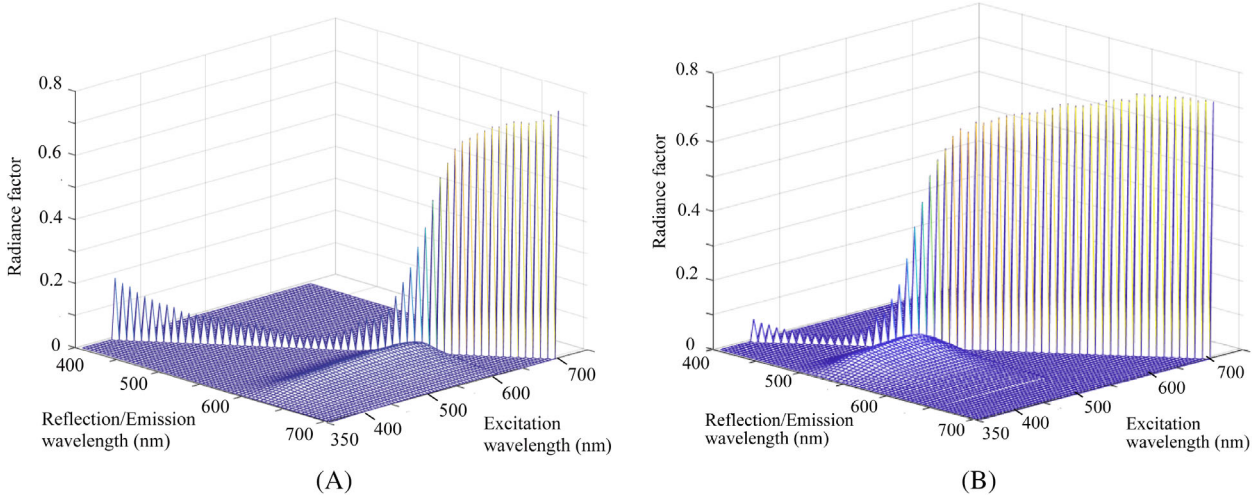

FIGURE 3 Donaldson matrices obtained from (A) the red fluorescent object on the left of Figure 1 and (B) the yellow fluorescent object on the right. The vertical axes indicate spectral radiance factors. The diagonal elements correspond to the surface-spectral reflectances that produce red and yellow colors, respectively. The humps in the emission wavelength ranges of 600 to 700 nm and 500 to 600 nm represent the luminescent radiance factors that produce orange and green colors, respectively

analyzed the angular dependency of the luminescence radiance factor in gonio-spectral measurements, showing that the radiance factor can be described using the Lambertian model. Thus, the fluorescent emission obeys Lambert's cosine law in the same way as the ideal diffuse reflection from a Lambertian diffuse surface.

As the first step for modeling the image formation, we assume two matte objects without fluorescence. The spectral radiance observed at each surface is described as

$$y_i(\mathbf{x},\lambda_{\mathrm{em}}) = f_{i1}(\mathbf{x})\,S_i(\lambda_{\mathrm{em}})E(\lambda_{\mathrm{em}}) + f_{i2}(\mathbf{x})\,S_i(\lambda_{\mathrm{em}})S_j(\lambda_{\mathrm{em}})E(\lambda_{\mathrm{em}}), \tag{3}$$

where $(i = 1, j = 2)$ or $(i = 2, j = 1)$. The first term on the right-hand side represents the diffuse reflection component directly reflected from each surface illuminated by a light source, and the second term represents the interreflection, where $S_i(\lambda_{\mathrm{em}})S_j(\lambda_{\mathrm{em}})$ is the spectral component of a single bounce of indirect illumination between the two surfaces.

Next, we assume two diffuse surfaces with fluorescence. The spectral radiance observed from each surface, accounting for mutual illumination, can be described by the following equations:

$$\begin{aligned} y_i(\mathbf{x},\lambda_{\mathrm{em}}) = {} & f_{i,\mathrm{re}}(\mathbf{x})\,S_i(\lambda_{\mathrm{em}})E(\lambda_{\mathrm{em}}) \\ & + f_{i,\mathrm{rr}}(\mathbf{x})\,S_i(\lambda_{\mathrm{em}})S_j(\lambda_{\mathrm{em}})E(\lambda_{\mathrm{em}}) \\ & + f_{i,\mathrm{le}}(\mathbf{x})\,C_{i1}(\lambda_{\mathrm{em}})\,\alpha_i(\lambda_{\mathrm{em}}) \\ & + f_{i,\mathrm{lr}}(\mathbf{x})\,C_{i2}(\lambda_{\mathrm{em}})\,\alpha_i(\lambda_{\mathrm{em}}) \\ & + f_{i,\mathrm{ll}}(\mathbf{x})\,C_{i3}(\lambda_{\mathrm{em}})\,\alpha_i(\lambda_{\mathrm{em}}) \\ & + f_{i,\mathrm{rl}}(\mathbf{x})\,C_{i4}(\lambda_{\mathrm{em}})\,S_i(\lambda_{\mathrm{em}})\,\alpha_j(\lambda_{\mathrm{em}}) \end{aligned} \tag{4}$$

where $(i = 1, j = 2)$ or $(i = 2, j = 1)$,

$$\begin{aligned} C_{i1}(\lambda_{\mathrm{em}}) &= \int_{350}^{\lambda_{\mathrm{em}}} \beta_i(\lambda_{\mathrm{ex}})E(\lambda_{\mathrm{ex}})d\lambda_{\mathrm{ex}} \\ C_{i2}(\lambda_{\mathrm{em}}) &= \int_{350}^{\lambda_{\mathrm{em}}} \beta_i(\lambda_{\mathrm{ex}})S_j(\lambda_{\mathrm{ex}})E(\lambda_{\mathrm{ex}})d\lambda_{\mathrm{ex}} \\ C_{i3}(\lambda_{\mathrm{em}}) &= \int_{350}^{\lambda_{\mathrm{em}}} \beta_i(\lambda_{\mathrm{ex}})\alpha_j(\lambda_{\mathrm{ex}})\left(\int_{350}^{\lambda_{ex}} \beta_j(\lambda'_{\mathrm{ex}})E(\lambda'_{\mathrm{ex}})d\lambda'_{\mathrm{ex}}\right)d\lambda_{\mathrm{ex}} \\ C_{i4}(\lambda_{\mathrm{em}}) &= \int_{350}^{\lambda_{\mathrm{em}}} \beta_j(\lambda_{\mathrm{ex}})E(\lambda_{\mathrm{ex}})d\lambda_{\mathrm{ex}} \end{aligned} \tag{5}$$

The spectral radiance is represented as a linear combination of six spectral functions: (1) diffuse reflection on a matte surface by direct illumination from a light source, (2) diffuse-diffuse interreflection between two matte surfaces, (3) luminescence caused by excitation based on direct illumination from a light source, (4) luminescence caused by reflected light from another surface, (5) luminescence caused by fluorescent illumination from another surface, and (6) interreflection caused by fluorescent illumination from another surface. The subscripts re, rr, le, lr, ll, and rl of the shading terms in Equation (4) correspond to the above components (1), (2), (3), (4), (5), and (6), respectively. Note that component (5) is present only if the excitation spectrum on one surface has a longer wavelength than the emission spectrum on another surface, that is, $\alpha_2(\lambda) < \beta_1(\lambda)$ or $\alpha_1(\lambda) < \beta_2(\lambda)$. The spectral functions $C_{i1}(\lambda)$, $C_{i2}(\lambda)$, and $C_{i3}(\lambda)$ are constant in the longer wavelength range, with $\beta_i(\lambda) = 0$, and the emission function $\alpha_i(\lambda)$ is quite small in the lower wavelength range. Figure 4 shows the spectral functions $C_{i1}(\lambda)$, $C_{i2}(\lambda)$, and $C_{i3}(\lambda)$ for the red fluorescent object $(i = 1)$ on the left of Figure 1 and the yellow fluorescent object $(i = 2)$ on the right. As a result, the third, fourth, and fifth terms in Equation (4) have the same spectral shape (see Reference 8). Therefore, we can merge such terms into one luminescence function given by $C_{i1}(\lambda) + C_{i2}(\lambda) + C_{i3}(\lambda)$, such that the spectral composition is described using four spectral components.

2.4 | Appearance decomposition of two fluorescent objects

The spectral model in Equation (4) can be represented in a discrete form to reduce computational complexity, in particular because MATLAB uses optimized routines that leverage SIMD operations. Let $\mathbf{s}_i$ $(i = 1, 2)$ and $\boldsymbol{\alpha}_i$ $(i = 1, 2)$ be n-dimensional column vectors representing the reflectance and emission spectra of surface i, respectively. Let $\mathbf{c}_{i1}$ and $\mathbf{c}_{i2}$ $(i = 1, 2)$ be n-dimensional column vectors

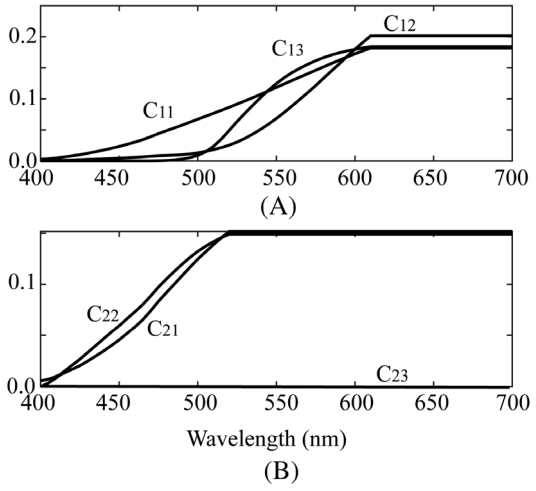

FIGURE 4 Spectral functions $C_{i1}(\lambda)$, $C_{i2}(\lambda)$, and $C_{i3}(\lambda)$ for the fluorescent objects in Figure 1, where (A) represents the red fluorescent object $(i = 1)$ and (B) represents the yellow fluorescent object $(i = 2)$

corresponding to $C_{i1}(\lambda)+C_{i2}(\lambda)+C_{i3}(\lambda)$ and $C_{i4}(\lambda)$ in Equation (5). All spectral functions are summarized into $n \times 4$ matrices $\mathbf{A}_i$ $(i = 1, 2)$ as follows:

$$\begin{aligned}\mathbf{A}_1 &\equiv [\mathbf{a}_{11}\ \mathbf{a}_{12}\ \mathbf{a}_{13}\ \mathbf{a}_{14}] = [\mathbf{s}_1.*\mathbf{e}\ \ \mathbf{s}_1.*\mathbf{s}_2.*\mathbf{e}\ \ \mathbf{c}_{11}.*\boldsymbol{\alpha}_1\ \ \mathbf{c}_{12}.*\mathbf{s}_1.*\boldsymbol{\alpha}_2] \\ \mathbf{A}_2 &\equiv [\mathbf{a}_{21}\ \ \mathbf{a}_{22}\ \ \mathbf{a}_{23}\ \ \mathbf{a}_{24}] = [\mathbf{s}_2.*\mathbf{e}\ \ \mathbf{s}_1.*\mathbf{s}_2.*\mathbf{e}\ \ \mathbf{c}_{21}.*\boldsymbol{\alpha}_2\ \ \mathbf{c}_{22}.*\mathbf{s}_2.*\boldsymbol{\alpha}_1]\end{aligned}, \tag{6}$$

where $\mathbf{e}$ represents an n-dimensional column vector of the illuminant $E(\lambda)$, and the symbol .* represents element-wise multiplication. Let $\mathbf{f}_i(\mathbf{x})$ $(i = 1, 2)$ be 4-dimensional column vectors representing the shading terms at position $\mathbf{x}$ of surface i, which can be used as weights for the spectral components.

$$\begin{aligned}\mathbf{f}_1(\mathbf{x}) &\equiv [f_{11}(\mathbf{x})\ \ f_{12}(\mathbf{x})\ \ f_{13}(\mathbf{x})\ \ f_{14}(\mathbf{x})]^t \\ \mathbf{f}_2(\mathbf{x}) &\equiv [f_{21}(\mathbf{x})\ \ f_{22}(\mathbf{x})\ \ f_{23}(\mathbf{x})\ \ f_{24}(\mathbf{x})]^t\end{aligned}, \tag{7}$$

where the apex t represents the matrix transposition. Furthermore, let $\mathbf{y}_i(\mathbf{x})$ $(i = 1, 2)$ be n-dimensional observation vectors representing $[y_i(\mathbf{x},\lambda_1)\ \ y_i(\mathbf{x},\lambda_2)\ \ \cdots\ \ y_i(\mathbf{x},\lambda_n)]^t$. Then, the spectral model of the observations with mutual illumination can be represented by a simple matrix equation as

$$\mathbf{y}_1(\mathbf{x}) = \mathbf{A}_1\mathbf{f}_1(\mathbf{x}),\ \ \mathbf{y}_2(\mathbf{x}) = \mathbf{A}_2\mathbf{f}_2(\mathbf{x}). \tag{8}$$

In the above representation, we note that the luminescence components $f_{i3}(\mathbf{x})\mathbf{a}_{i3}(\lambda)$ $(i = 1, 2)$ arise from two different optical processes. The first one is emissions excited by direct illumination from the light source, and the other is emissions excited by the reflection and emission light from another surface. In other words, the first type of luminescence is caused by direct illumination, while the rest is caused by indirect illumination.

As described in Section 2.3, the fluorescent emission obeys Lambert's cosine law in the same way as the ideal diffuse reflection from a Lambertian diffuse surface. Therefore, the two types of fluorescent emission (caused by direct and indirect illuminations) correspond to the diffuse reflection by direct illumination and the diffuse-diffuse interreflection, and their spatial distributions also correspond.

The luminescence shading terms $f_{i3}(\mathbf{x})$ $(i = 1, 2)$ can be further decomposed into the direct and indirect illumination components as follows:

$$f_{i3}(\mathbf{x}) = c_{i1}f_{i1}(\mathbf{x}) + c_{i2}f_{i2}(\mathbf{x}), (i = 1, 2) \tag{9}$$

where $f_{i1}(\mathbf{x})$ and $f_{i2}(\mathbf{x})$ are the shading terms of the diffuse reflection and the diffuse-diffuse interreflection, respectively, in Equation (7), and the symbols c_1 and c_2 are the weighting coefficients. The benefit of this decomposition is the ability to analyze the generation process of the luminescence geometrically. Although the spectral compositions of the two components are identical, the generation processes are different. The weights are determined using a standard least-squares method.

Finally, the spectral model for the radiance observed from two fluorescent objects with mutual illumination effects can be composed of five physical components: (1) diffuse reflection, (2) diffuse-diffuse interreflection, (3) luminescence excited by direct illumination, (4) luminescence excited by indirect illumination, and (5) interreflection caused by fluorescent illumination. Appearance decomposition is mathematically described as follows:

$$\begin{aligned}\mathbf{y}_i(\mathbf{x}) &= f_{i1}(\mathbf{x})\mathbf{a}_{i1} + f_{i2}(\mathbf{x})\mathbf{a}_{i2} + \cdots + f_{i5}(\mathbf{x})\mathbf{a}_{i5} \\ &= \mathbf{A}_i\mathbf{f}_i(\mathbf{x})\end{aligned}, (i = 1, 2) \tag{10}$$

where the spectral matrices $\mathbf{A}_i$ are defined as

$$\begin{aligned}\mathbf{A}_1 &= [\mathbf{s}_1.*\mathbf{e}\ \ \mathbf{s}_1.*\mathbf{s}_2.*\mathbf{e}\ \ \mathbf{c}_{11}.*\boldsymbol{\alpha}_1\ \ \mathbf{c}_{11}.*\boldsymbol{\alpha}_1\ \ \mathbf{c}_{12}.*\mathbf{s}_1.*\boldsymbol{\alpha}_2] \\ \mathbf{A}_2 &= [\mathbf{s}_2.*\mathbf{e}\ \ \mathbf{s}_1.*\mathbf{s}_2.*\mathbf{e}\ \ \mathbf{c}_{21}.*\boldsymbol{\alpha}_2\ \ \mathbf{c}_{21}.*\boldsymbol{\alpha}_2\ \ \mathbf{c}_{22}.*\mathbf{s}_2.*\boldsymbol{\alpha}_1]\end{aligned} \tag{11}$$

Although the third and fourth columns in the spectral matrices are coincident, $\mathbf{a}_{i3} = \mathbf{a}_{i4}$, the shading terms are different: $f_{i3}(\mathbf{x}) \neq f_{i4}(\mathbf{x})$ $(i = 1, 2)$. Descriptive subscripts rather than numbers may be helpful. In this case, the subscripts of re, rr, le, li, and rl are used as in the shading terms $f_{i,\mathrm{re}}(\mathbf{x})$, $f_{i,\mathrm{rr}}(\mathbf{x})$, $f_{i,\mathrm{le}}(\mathbf{x})$, $f_{i,\mathrm{li}}(\mathbf{x})$, and $f_{i,\mathrm{rl}}(\mathbf{x})$, corresponding to the components (1), (2), (3), (4), and (5), respectively.

Figure 5 demonstrates the appearance decomposition for a scene with two fluorescent objects with matte surfaces, as shown in Figure 1, where the acquired image is linearly decomposed into five components according to the above decomposition procedure.

3 | APPEARANCE SYNTHESIS BASED ON A PHYSICALLY BASED SIMULATION

3.1 | Principle of appearance synthesis

The shading terms, depending on the object surface geometry and position, are crucial for the appearance reconstruction of fluorescent objects under different conditions. If two objects have planar and matte surfaces, the shading terms may be estimated under some restrictions using an image-based approach without 3D shape data.[10]

We acquired multiple images of the same object under a directional light source by changing the illumination direction. Then, the surface normal vector on the surface geometry can be estimated using a photometric stereo method, which is based on the shading change under illumination direction. The shading terms can be predicted so that the appearance of the object is reconstructed in an arbitrary illumination direction.

Because we consider the appearance synthesis for fluorescent objects with complex and realistic shapes, the aforementioned image-based approach for flat surfaces cannot be used to determine the shading terms. Recall that the luminescent component of a fluorescent object is emitted uniformly in all directions, so that it can be approximated as a perfect diffuser. Therefore, we can assume that $f_{i,\mathrm{re}}(\mathbf{x}) = f_{i,\mathrm{le}}(\mathbf{x})$ and $f_{i,\mathrm{rr}}(\mathbf{x}) = f_{i,\mathrm{li}}(\mathbf{x}) = f_{i,\mathrm{rl}}(\mathbf{x})$ ($i = 1, 2$). As a result, estimating the initial five factors can be reduced to estimate only two shading terms, $f_{i,\mathrm{re}}(\mathbf{x})$ and $f_{i,\mathrm{rr}}(\mathbf{x})$, a direct and indirect reflection term. In other words, the shading terms for the fluorescent components can be obtained from the reflection components.

This result motivates the adoption of a physically based simulation approach: a standard renderer can be used to simulate the physical interreflection phenomena between reflecting objects with arbitrary shapes. We note that because the shading terms include brightness information, these terms depend not only on geometries, but also on spectral functions. Figure 5 depicts the basic process of the appearance synthesis.

First, suppose that two matte objects closely placed under uniform illumination are nonfluorescent. The 3D shape data, spectral reflectance data, illuminant data, and proper locations of the light source and camera are provided as the input data for spectral rendering in the visible wavelength range. The output spectral image is linearly decomposed into the two components of diffuse reflection and interreflection as follows:

$$\mathbf{y}_i(\mathbf{x}) = f_{i,re}(\mathbf{x})\mathbf{a}_{i1} + f_{i,rr}(\mathbf{x})\mathbf{a}_{i2}, (i = 1, 2) \tag{12}$$

where $\mathbf{a}_{i1} = \mathbf{s}_i.*\mathbf{e}$ and $\mathbf{a}_{i2} = \mathbf{s}_i.*\mathbf{s}_j.*\mathbf{e}$. The shading factors $f_{i,\mathrm{re}}(\mathbf{x})$ and $f_{i,\mathrm{rr}}(\mathbf{x})$ ($i = 1, 2$) for the two components are estimated at every pixel position from the observed spectral image using the standard linear least-squares optimization.

Second, the estimated shading factors $f_{i,\mathrm{re}}(\mathbf{x})$ and $f_{i,\mathrm{rr}}(\mathbf{x})$ are available for the shading factors $f_{i,\mathrm{le}}(\mathbf{x})$, $f_{i,\mathrm{li}}(\mathbf{x})$, and $f_{i,\mathrm{rl}}(\mathbf{x})$ of the fluorescent components. Because fluorescence emission is based on excitation over UV and visible wavelengths, the three spectral functions $\mathbf{a}_i$ ($i = 3, 4, 5$) are calculated from the excitation spectrum $\beta(\lambda)$, the emission spectrum $\alpha(\lambda)$, and the spectral reflectance $S(\lambda)$ of each object, and the illuminant $E(\lambda)$ in the broad wavelength range. (Refer to Equations (4) and (5) for the calculations.)

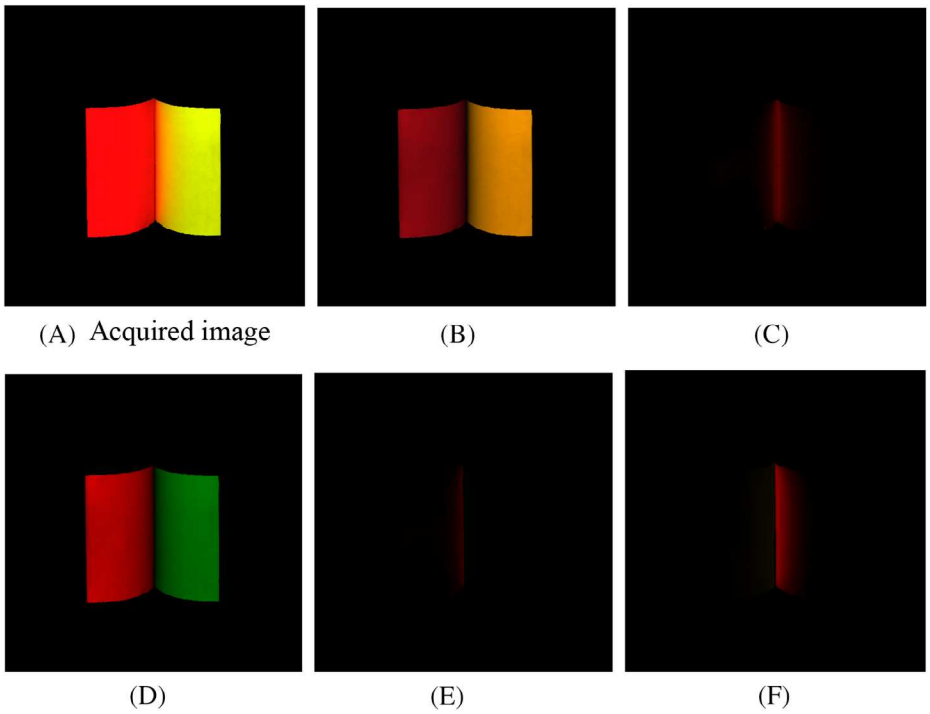

FIGURE 5 The acquired image in Figure 1, shown here as (A), has been decomposed into five components (see text for more details): (B) diffuse reflection, (C) interreflection, (D) luminescence by direct illumination, (E) luminescence by indirect illumination, and (F) interreflection by fluorescent illumination. These images were obtained from the spectral data using the CIE-XYZ to sRGB transformation (see Section 3.4)

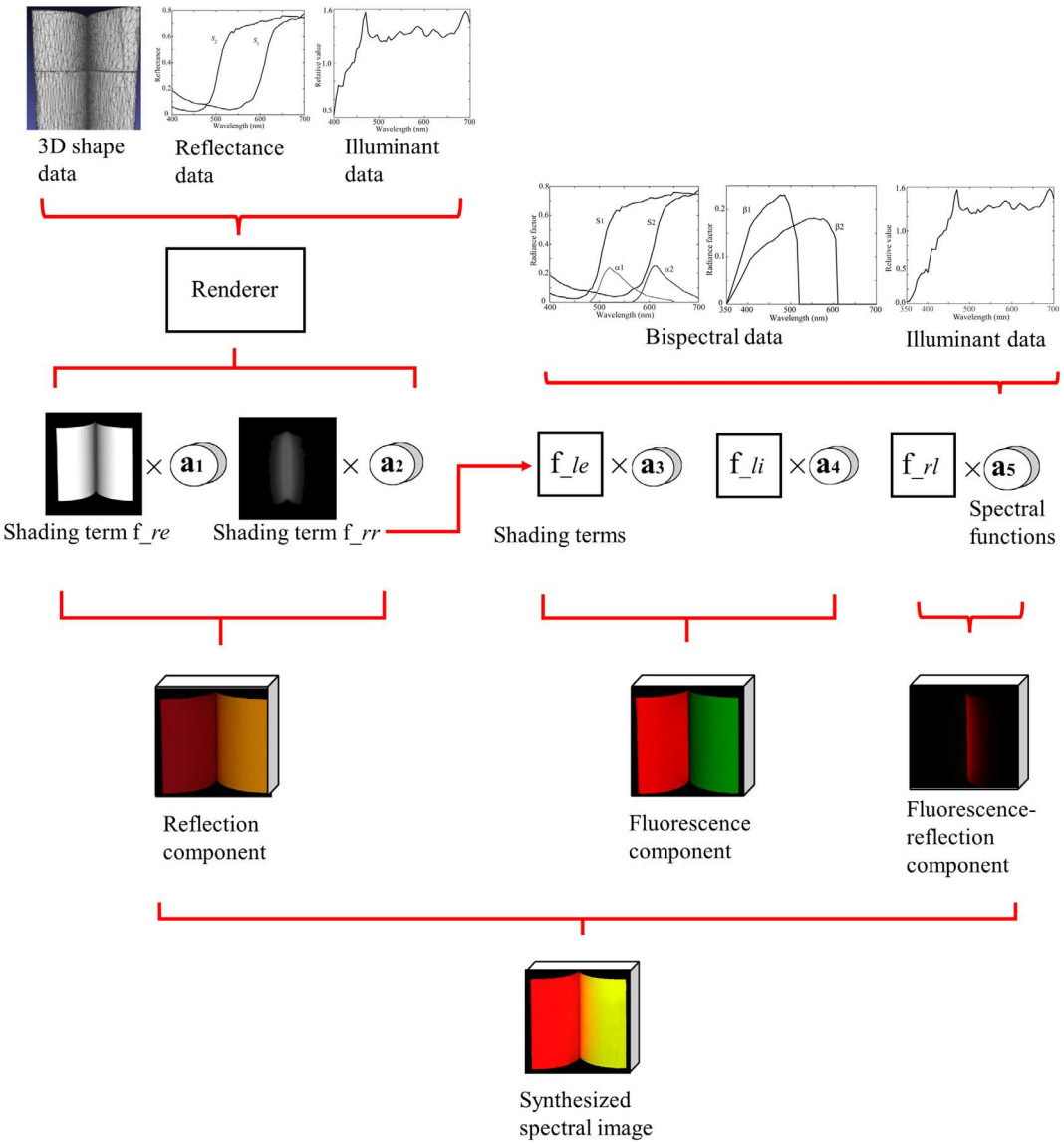

FIGURE 6 Basic process of the spectral appearance synthesis (refer to Section 3.1 for details of the shading terms)

Among the five components, the first two are reflection components. The third and fourth are the fluorescence emission components. The fifth component is the reflection component due to fluorescence emission. The overall appearance of the target fluorescent objects is obtained by synthesizing these components as a linear sum.

3.2 | Simulation settings

The physically based simulation used to estimate the reflection components of the diffuse reflection is based on the Monte Carlo simulation to trace the paths of photons, both starting from the light source and from the image sensor (bidirectional path tracer). In this study, we make use of the physically-based spectral renderer Mitsuba v0.6.[24]

The "bdpt" bidirectional path tracer is used in this study. Its main parameters are the longest path depth ("maxDepth") and the minimum path depth to use the Russian roulette termination criterion ("rrDepth"). The latter is used to terminate the long path (ie, above some threshold), while compensating for the bias that would otherwise be introduced.[25] In a real scene, the interreflection can be estimated according to infinite bounces. Therefore, we set "maxDepth" to "−1" corresponding to ∞ bounces. We set the "rrDepth" value to "10."

The 3D shape data of the objects, acquired by means of a 3D scanner, are input as OBJ files. The BRDF of the material is set to perfect diffusion. The spectral functions of reflectance and illuminant are represented in 5 nm

intervals in the wavelength range of 400 to 700 nm. We assume directional illumination with parallel beams. A perspective camera model is used, setting its field of view so that the rendered image fits the acquired image. The location and orientation of the camera and lighting are adjusted to match real images. We use the "independent" sampler, using 1024 samples per pixel. Finally, the output image, of size 512-by-512 pixels, is rendered spectrally and saved as a MATLAB M-file.

Using the above settings, the image of the reflection component, including the interreflection, is rendered. Figure 7 shows the rendered reflection image for the two fluorescent half-cylinders in Figure 1, where the fluorescent components are not included. The spectral image is then decomposed into the diffuse reflection component and the interreflection component based on the spectral functions $(\mathbf{s}_1.*\mathbf{e}, \mathbf{s}_2.*\mathbf{e})$ and $\mathbf{s}_1.*\mathbf{s}_2.*\mathbf{e}$ to estimate the corresponding shading factors.

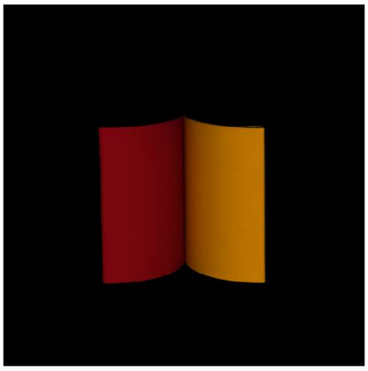

FIGURE 7 Rendered image of the reflection component including interreflection for the two fluorescent half-cylinders in Figure 1. The 3D data of the two fluorescent half-cylinders, the spectral reflectance data of the two objects, and the illuminant spectral data of the artificial sunlight were used in rendering, where the image size was standardized to 512-by-512 pixels. Both camera and lighting location and direction were adjusted to match the real scene

FIGURE 8 Acquired image of two half-cylindrical objects placed in contact, the materials of which are pink and orange matte papers without fluorescence

3.3 | Correction using image data

The Monte Carlo simulation might not produce interreflections that match the measured data. In our experiments, the intensity of the interreflection in the rendered image was often lower than the intensity in the real images. Possible reasons for such a mismatch may include the following:

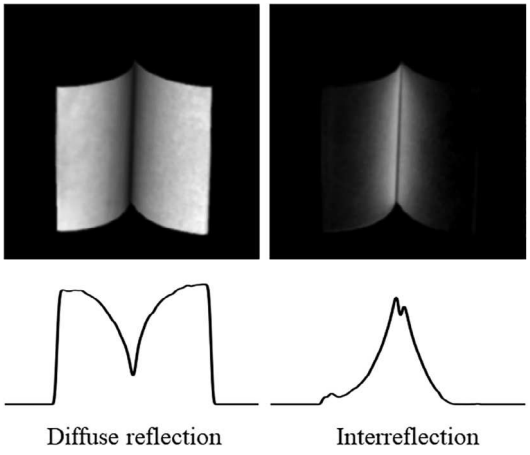

FIGURE 9 Two images of the shading terms $f_1(\mathbf{x})$ and $f_2(\mathbf{x})$, derived from the acquired image in Figure 8, respectively for diffuse reflection and interreflection, where the lower graphs represent the intensity profiles in horizontal cross-section

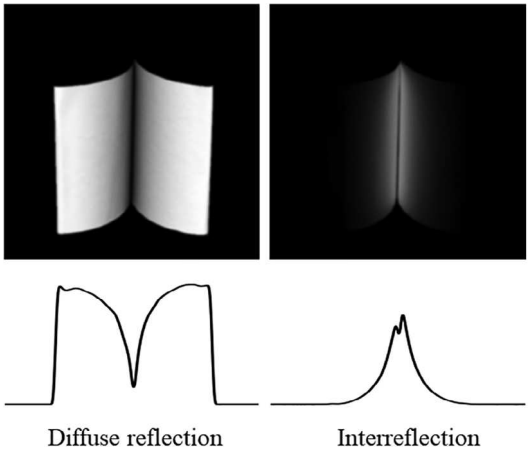

FIGURE 10 Two images of shading terms $f_1'(\mathbf{x})$ and $f_2'(\mathbf{x})$ of the diffuse reflection and interreflection predicted by the simulation of infinite bounces between the two surfaces, where the graphs represent the intensity profiles in horizontal cross-sections

1. Imperfect captured geometry. Even though we use measured data for the 3D shapes, scanned at high resolution, the number of polygons is still finite.
2. Inaccuracies of the BRDF model.[26] As often pointed out, there is no perfect Lambertian material in reality.
3. The simulated lighting is not perfectly aligned with the real conditions.
4. The simplified assumption of single-reflection for the interreflection term.

In the following, we present a simple method to compensate for the difference between the measured and simulated interreflections. Figure 8 shows an actual sample image used for the explanation, where the two half-cylindrical objects are placed in contact, the materials of which are pink and orange matte papers without fluorescence. The objects were measured using a spectral imaging system under artificial sunlight illumination. The captured spectral image was decomposed into two components, diffuse reflection and interreflection, based on knowledge of the spectral functions, where the spectral reflectances and the illuminant spectrum were measured separately. Figure 9 shows two images of the shading terms $f_1(\mathbf{x})$ and $f_2(\mathbf{x})$ for diffuse reflection and interreflection. In the figure, the lower graphs represent the intensity profiles in the horizontal cross-section.

The spectral image rendered in Mitsuba was obtained using scanned 3D shape data, setting the scene and renderer parameters to match the real conditions as closely as possible. The rendered spectral image was decomposed into two components using the same spectral functions as earlier. Figure 10 shows the shading terms $f_1'(\mathbf{x})$ and $f_2'(\mathbf{x})$ of the diffuse reflection and interreflection predicted by the simulation of infinite bounces between the two surfaces. Note that the shading term images in Figures 9 and 10 are normalized so that the averaged intensities $\overline{f_1(\mathbf{x})}$ and $\overline{f_1'(\mathbf{x})}$ of the diffuse reflection are coincident as $\overline{f_1(\mathbf{x})} = \overline{f_1'(\mathbf{x})}$ between the two images. We note that the intensity of the interreflection component $f_2'(\mathbf{x})$ predicted from the simulation is lower than that estimated from the real image of the same object, $f_2(\mathbf{x})$. Figure 11 compares the profiles of $f_2'(\mathbf{x})$ and $f_2(\mathbf{x})$ side-by-side.

FIGURE 11 Comparison of the profiles of shading terms $f_2(\mathbf{x})$ and $f_2'(\mathbf{x})$ for the interreflection in Figures 9 and 10

Because the shading terms assume relative values, we calculate the relative intensities of the shading terms averaged over an area where the two objects are close to each other. Then, we set $w = \overline{f_2(\mathbf{x})}/\overline{f_1(\mathbf{x})}$ and $w' = \overline{f_2'(\mathbf{x})}/\overline{f_1'(\mathbf{x})}$. The ratio of these values can be used as a compensation factor to correct shading terms in the simulation image. The shading terms in the appearance synthesis process in Figure 4 are then corrected as:

$$f_2(\mathbf{x}) = f_4(\mathbf{x}) = f_5(\mathbf{x}) = (w/w')f_2'(\mathbf{x}), \tag{13}$$

where $\overline{f_1(\mathbf{x})} = \overline{f_3(\mathbf{x})} = \overline{f_1'(\mathbf{x})}$.

3.4 | Evaluation of synthesized appearance

Because the resulting synthesized appearance is represented by high-dimensional spectral images, the appearance quality can be properly evaluated on a calibrated display device. On a standard sRGB display, all spectral images are first transformed into CIE-XYZ images using the CIE color-matching functions and then converted into sRGB images.

To evaluate our results objectively, we introduce performance-index functions to assess the accuracy of the proposed synthesis method. In particular, the metrics of (1) spectral angle and (2) color difference are used to investigate the differences between the synthesized images and the corresponding real images used as ground truth.

The spectral angle was originally used for the classification of high-dimensional image data captured by a hyperspectral imaging system in the field of remote sensing.[27] It computes the spectral similarity between the image and the reference spectra. The basic formula of the spectral angle represents the angle between two vectors in a high-dimensional spectral space, defined as follows:

$$\theta = \cos^{-1}\left(\frac{\mathbf{y}.^{*}\mathbf{y}'}{\|\mathbf{y}\|\|\mathbf{y}'\|}\right), \tag{14}$$

where the symbol $\|\mathbf{y}\|$ indicates the norm $\mathbf{y}$. The angle θ represents the spectral similarity of $\mathbf{y}$ and $\mathbf{y}'$. As the spectral angle decreases, the two vectors become more similar. The angle ranges from 0° to 90°. This metric is not affected by the illumination intensity because the angle between the two vectors is independent of the norm of the vectors. We calculated the spectral angle at each pixel between the synthesized and real images.

As for the color difference, it is noteworthy that approximately perceptually uniform color spaces such as the CIELAB color space are not available for fluorescent

colors because they are defined on object colors by diffuse reflection. Therefore, we use the color difference on the 3D color space of sRGB, which is formulated as

$$\Delta\text{sRGB} = \sqrt{(R-R')^2+(G-G')^2+(B-B')^2}, \qquad (15)$$

where $0 \le R, G, B \le 1$. This color difference is in the ranges $[0, \sqrt{3}]$. This metric is useful for most displays in the sRGB standard.

When calculating the spectral angle and the color difference, we should note a registration error between the synthesized and acquired images. The acquired images have different sizes, and there is a slight difference between the simulated and real images. The registration error is corrected using the MATLAB commands "imregtform" and "imwarp" based on an affine transformation.

4 | RESULTS

4.1 | Results of appearance synthesis

First, the spectral appearance of sharp concave surfaces, given by two cylindrical objects placed next to each other (Figure 1), was synthesized according to the process depicted in Figure 6. The spectral image rendered in Mitsuba using the shape and spectral data, setting the scene parameters to match the real conditions, was decomposed into two components: diffuse reflection and interreflection. We also obtained the shading terms for diffuse reflection and interreflection from the decomposition of the real spectral image. The shading terms between the simulation and real cases were compared using the method described in Section 3.3. As a result, the correction coefficient ($w/w' = 1.49$) was applied to the interreflection component obtained by the simulation. Figure 12 shows the shading terms of the two components by simulation with the correction. These were used as the shading terms $f_{\_\mathrm{le}}(\mathbf{x})$, $f_{\_\mathrm{li}}(\mathbf{x})$, and $f_{\_\mathrm{rl}}(\mathbf{x})$ for synthesizing the fluorescent components. The spectral functions $\mathbf{a}_i$ ($i = 3, 4, 5$) were calculated from the Donaldson matrices reported in Figure 3 and the illuminant spectrum shown in Figure 2. Figure 13 (top row) shows the component images (1)-(5) produced by multiplying the shading terms and the spectral functions in each step of the appearance synthesis process. For comparison, the five component images derived from the acquired image (see Figure 5) are shown in the bottom row. Figure 14 shows the color image resulting from the spectral appearance synthesis, given by the linear sum of the five components; for comparison, the acquired image is reported on the right side.

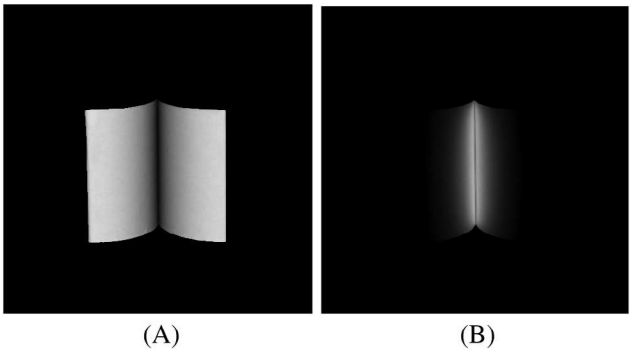

FIGURE 12 Shading terms for the two components of (A) diffuse reflection and (B) interreflection obtained by the simulation with correction

Next, we demonstrate the results of its application to other fluorescent objects. Figure 15 shows the acquired color image of another scene using the spectral imaging system, in which a curved object is placed on a plane. The diffuse color of the curved object is pink, with a red fluorescence color, whereas the plane is green and displays a more saturated green fluorescence color. Mutual illumination appears at the boundary area where the two objects are in contact. The Donaldson matrix of each object in a scene composed of a curved object and a flat plane supporting it was reported in.[10] The illumination is the same as that shown in Figure 2. The spectral image rendered in Mitsuba by setting the scene parameters to match the real conditions was decomposed into diffuse reflection and interreflection components based on the spectral functions. The real spectral image was also decomposed. The shading terms for diffuse reflection and interreflection components were compared between the simulation and real cases in the front area of the scene in Figure 15, where the two objects are in contact and mutual reflection occurs. The correction coefficient was $(w/w) = 1.61$. Figure 16 shows the shading terms of the two components by simulation with the correction. Figure 17 shows the component images (1)-(5) produced in each step of the appearance synthesis process, where the top row is relative to the synthesized image and the bottom row is obtained from the acquired image. Figure 18 shows the synthesized appearance resulting from the linear sum of the five component images, where the acquired image in Figure 15 is shown on the right side for comparison.

4.2 | Performance evaluation

We first compare the component images of the synthesized and acquired scenes, as shown in Figure 13, where

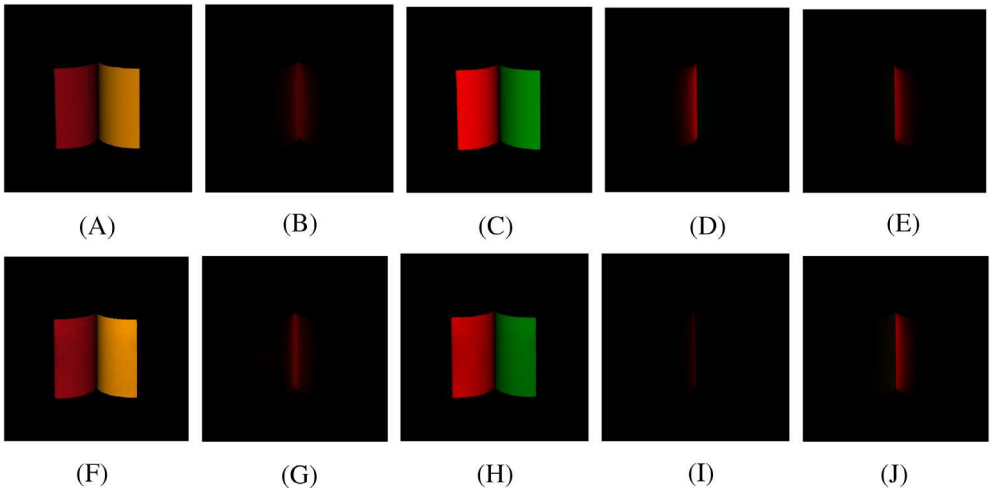

FIGURE 13 Component images produced in the appearance synthesis process of the sharp concave surfaces as in acute angle by two half-cylindrical objects: diffuse reflection (A,F), interreflection (B,G), luminescence by direct illumination (C,H), luminescence by indirect illumination (D,I), and interreflection by fluorescent illumination (E,J). The top row is derived from the synthesized image, whereas the bottom row is derived from the acquired image

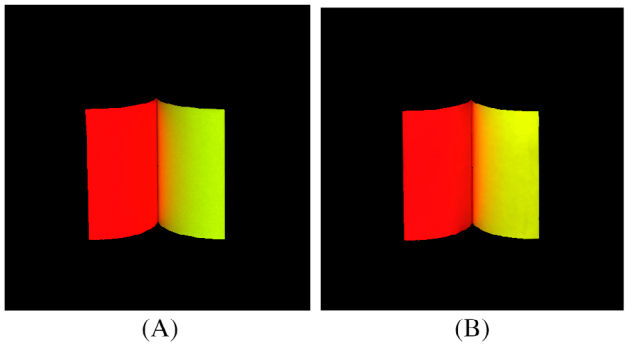

FIGURE 14 (A) Color image of the synthesized spectral appearance for the sharp concave surfaces by the linear sum of the five component images (see Figure 13A-E) and (B) acquired color image from the real scene (see Figure 1)

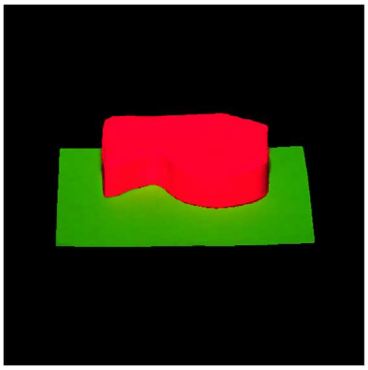

FIGURE 15 Acquired color image of the scene composed of a curved object and a flat plane supporting it

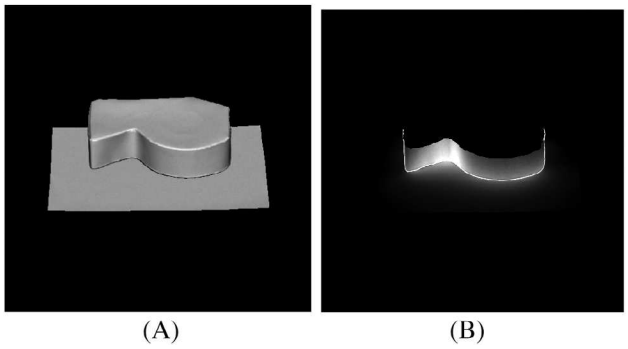

FIGURE 16 Shading terms for the two components of (A) diffuse reflection and (B) interreflection obtained by the simulation with the correction for the scene in Figure 15

the fourth component of the synthesized image (D), representing the luminescent component by indirect illumination, is stronger than the corresponding component obtained from the real image (I). In addition, a detailed inspection suggests that the third component image (C), representing the luminescent component by direct illumination, is slightly stronger than the corresponding component of the real image (H). These intensity differences affect the synthesized images. In Figure 14, there is a small color shift in the resulting object appearance in the right, which appears slightly greenish in the synthesized image and a little more reddish in the acquired image. Notably, the fifth component images (E) and (J) that the interreflection component caused by fluorescent illumination is quite small on the left object. This phenomenon can be explained using the Donaldson matrices, as shown in Figure 3. The fluorescent spectrum (green) emitted from the right object is shorter in the effective wavelength range than the spectral reflectance (orange) of the left object. Therefore, a minor color change occurred on the left object.

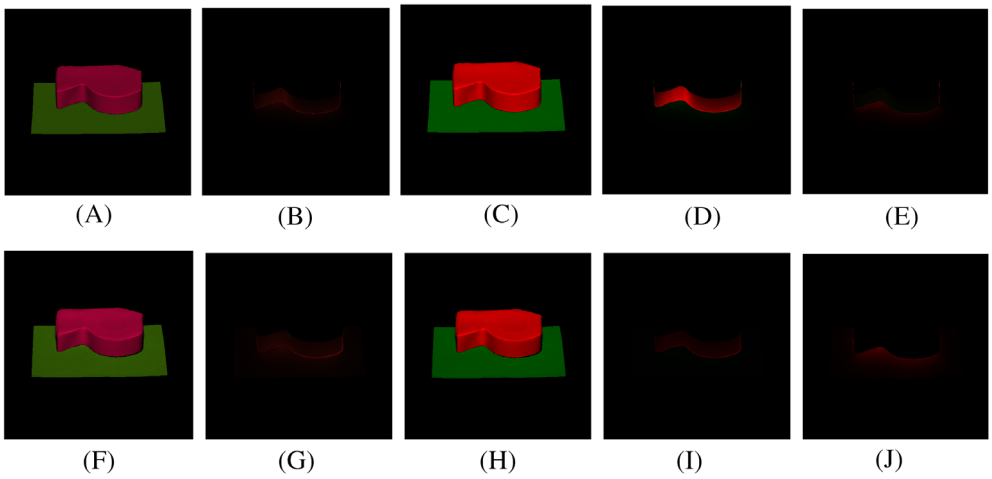

FIGURE 17 Component images produced in the appearance construction process for the scene of a curved object and a flat plane supporting it: diffuse reflection (A,F), interreflection (B,G), luminescence by direct illumination (C,H), luminescence by indirect illumination (D,I), and interreflection by fluorescent illumination (E,J). The top row refers to the synthesized image, whereas the bottom row refers to the acquired image

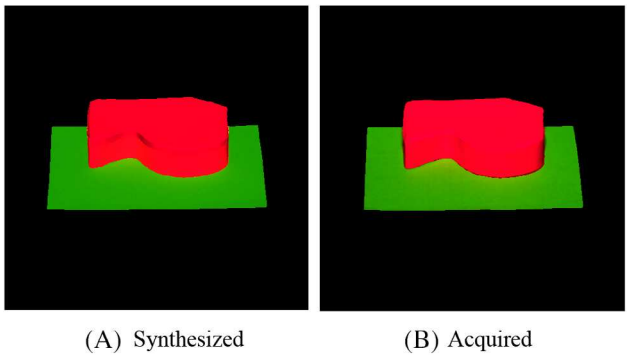

FIGURE 18 (A) Color image of the synthesized spectral appearance for the scene obtained as the linear sum of the five component images. (B) Acquired color image from the real scene (see Figure 15)

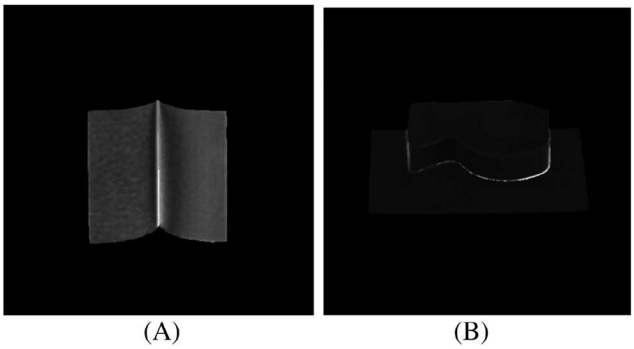

FIGURE 19 Spatial distributions of the spectral angle for (A) the sharp concave surfaces and (B) the surfaces of a curved object and a flat plane supporting it

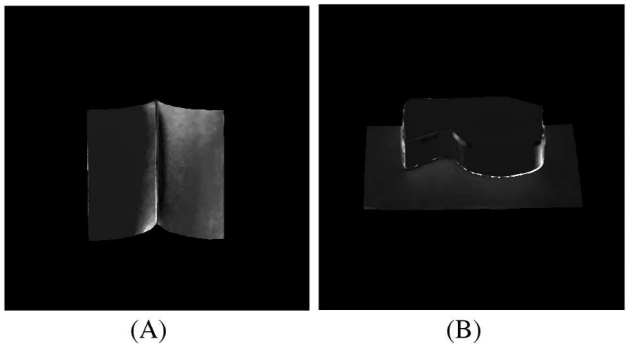

FIGURE 20 Spatial distributions of the sRGB color difference for (A) the sharp concave surfaces and (B) the surfaces of a curved object and a flat plane supporting it

As for the second set of objects, the comparison in Figure 18 suggests that the overall appearance of the curved object is well reproduced. Similar to the other scene, the comparison between the component images in Figure 17 shows that the fourth component of the synthesized image (D) is stronger than the corresponding component of the real image (I); the fifth component (E), representing interreflection by fluorescent illumination, is slightly weaker than the corresponding component of the real image (J).

Figure 19 shows the spatial distributions of the spectral angle for (A) sharp concave surfaces and (B) surfaces of a curved object and a flat plane supporting it. Figure 20 shows the spatial distributions of the color differences for the first and second scenes. The two metrics are represented in the grayscale of the range [0, 1], where the values 0 (black) and 1 (white) represent perfect recovery and nonperfect recovery, respectively. Numerically, on the angle scale, the minimum 0 and the

maximum 1 correspond to 0° and 90°, respectively. In the sRGB difference scale, those correspond to 0 and $\sqrt{3}$.

Inspection of Figure 19A,B suggests that large spectral angles are limited to the narrow areas where the two objects connect, whereas the angle is smaller in other areas. That is, the synthesized image is spectrally accurate. The average spectral angles are 2.41° and 3.33°, respectively, for the objects in Figure 19A and B, respectively. The standard deviations are 5.08° and 7.32°, respectively. Because the spectrum of mutual illumination is computed as a single bounce of indirect illumination, the spectral error increases in the connection areas between the objects.

Figure 20 shows that the color difference values distribution over the surface do not always assume larger values at the connection areas. Although the spectral angle does not contain intensity information because of its normalization, the sRGB color difference contains relative intensity information. The average color differences are 0.091 and 0.079, respectively, for the objects in Figure 20A,B. These are considered within tolerances in sRGB image reproduction. The standard deviations are 0.050 and 0.049, respectively. The color difference appears prominent in the right object in Figure 20A. This is because, as mentioned earlier, the fluorescent component in the synthesized image is estimated to be stronger for the right object than for the real scene.

5 | CONCLUSIONS

We have proposed an approach for the synthesis of fluorescent objects in the presence of mutual illumination. When the 3D shape data and fluorescent Donaldson matrices are known, a realistic scene appearance can be rendered under different conditions of illumination, viewing, and shape, for arbitrary fluorescent materials. Our approach relies on a physically based simulation, where the interaction between light and object materials is precisely simulated using a renderer.

We first described the foundation of the spectral appearance model of fluorescent objects. When two fluorescent matte objects were close to each other, the spectral image was formulated based on their spectral reflectance, excitation, emission, and illuminant spectrum. We showed that the appearance could be decomposed into five components for efficient evaluation in vector/matrix form, which could be further expanded into a multiplication of spectral functions and shading terms.

Then, an appearance synthesis method was proposed for rendering the appearance of 3D fluorescent objects with mutual illumination. Building upon the similarity between diffuse reflection and fluorescence emission, the shading terms for mutual illumination could be simplified to the reflection component only. Therefore, it did not require modification of a standard rendering system that targets nonfluorescent objects. The Mitsuba renderer was used to estimate the reflection components based on the underlying Monte Carlo simulation. The spectral computation of the fluorescent component was performed over a broad wavelength range over the UV and visible wavelengths. The intensity of the interreflection in the simulated image was often lower than the intensity in the real images. We addressed possible reasons for such a mismatch and a method for compensating for the difference between the simulated and real images.

Experiments were performed to demonstrate the effectiveness of the proposed approach. The accuracy of the proposed approach was experimentally confirmed using objects with different shapes and fluorescence in the presence of complex mutual illumination effects. The spectral angle and RGB color difference were used as the metrics in the accuracy assessment. A faithful color reproduction can be achieved through the spectral imaging, so that the synthesized image can be visually evaluated on a calibrated display or printer. An advantage of this method is that only a small amount of data is required and this is mostly due to the 3D shape data.

As future work, we may consider a detailed investigation of the potential reasons for the difference between rendered and real images, and the extension of the proposed approach to more complex geometry and illumination conditions.

ACKNOWLEDGMENTS

This work was supported by Japan Society for the Promotion of Science KAKENHI Grant Number JP20K11893. This work was also supported by the Grant N-288670 ("Spectraskin"), funded by the Research Council of Norway. The authors would like to thank the reviewers for the helpful comments on improving the article.

DATA AVAILABILITY STATEMENT

Author elects to not share data

ORCID

Shoji Tominaga https://orcid.org/0000-0001-6460-7694

REFERENCES

[1] Wyszecki G, Stiles WS. *Color Science: Concepts and Methods, Quantitative Data and Formulae*. New York: Wiley; 1982.

[2] Lakowicz JR. *Principles of Fluorescence Spectroscopy*. 3rd ed. Berlin: Springer; 2006.

[3] Donaldson R. Spectrophotometry of fluorescent pigments. *Br J Appl Phys*. 1954;5(6):210-214.

[4] Tominaga S, Hirai K, Horiuchi T. Estimation of bispectral Donaldson matrices of fluorescent objects by using two illuminant projections. *J Opt Soc Am A*. 2015;32(6):1068-1078.

[5] Hullin MB, Hankika J, Ajdin B, Seidel HP, Kautz J, Lensch HPA. Acquisition and analysis of bispectral bidirectional reflectance and reradiation distribution functions. *ACM Trans Graphics*. 2010;29(4):1-7. doi:10.1145/1778765.1778834
[6] Drew MS, Funt BV. Calculating surface reflectance using a single-bounce model of mutual reflection. *Proc Int Conf Comput Vis*. 1990;393-399.
[7] Deeb R, Muselet D, Hebert M, Tremeau A. Interreflections in computer vision: a survey and an introduction to spectral infinite-bounce model. *J Math Imag Vis*. 2018;60:661-680.
[8] Tominaga S, Kato K, Hirai K, Horiuchi T. Spectral image analysis of mutual illumination between florescent objects. *J Opt Soc Am A*. 2016;33(8):1476-1487.
[9] Tominaga, S., Kato, K., Hirai, K., Horiuchi, T., Appearance reconstruction of fluorescent objects for different materials and light source. *Proceedings of the 26th Color and Imaging Conference (CIC25)*; 2017; 34-39.
[10] Tominaga S, Hirai K, Horiuchi T. Spectral reconstruction of fluorescent objects with mutual illumination effects. *J Opt Soc Am A*. 2019;36(9):1512-1522.
[11] Tominaga, S., Hirai, K., Horiuchi, T., Appearance reconstruction of fluorescent objects based on reference geometric factors. *Proceedings of the 26th Color and Imaging Conference (CIC27)*; 2019; 393-398.
[12] Jung A, Hamika J, Dachsbacher C. Spectral mollification for bidirectional fluorescence. *Comput Graph Forum*. 2020;39(2):373-384.
[13] Tominaga S, Hirai K, Horiuchi T. Estimation of fluorescent Donaldson matrices using a spectral imaging system. *Opt Express*. 2018;26(2):2132-2148.
[14] CIE. Calibration methods and photo-luminescent standards for total radiance factor measurements. *CIE 182:2007*. Vienna: Commission Internationale de l'Eclairage; 2007. doi:10.1002/col.20407
[15] Gundlach D, Terstiege H. Problems in measurement of fluorescent materials. *Color Res Appl*. 1994;19(6):427-436.
[16] Mohammadi, M. Developing an imaging bi-spectrometer for fluorescent materials, PhD Dissertation, Chester F. Carlson Center for Imaging Science, RIT, 2009.
[17] Fu Y, Lam A, Kobashi Y, Sato I, Okabe T, Sato Y. Reflectance and fluorescent spectra recovery based on fluorescent chromaticity invariance under varying illumination. *Proceedings of IEEE Conference Computer Vision and Pattern Recognition*; IEEE; 2014:2171-2178.
[18] Blasinski H, Farrell J, Wandell B. Simultaneous surface reflectance and fluorescence spectra estimation. *IEEE Trans Image Process*. 2020;29:8791-8804.
[19] Tominaga S. Estimation of bispectral characteristics of fluorescent objects based on multispectral imaging data. *Optical Eng*. 2021;60(3):033102-1–0033102-14.
[20] Wilkie A, Weidlich A, Larboulette C, Purgathofer W. A reflectance model for diffuse fluorescent surfaces. *Proc Graphite*. 2006;321-328.
[21] Treibitz T, Murez Z, Mitchell BG, Kriegman D. Shape from fluorescence. *Proc Eur Conf Comput Vis*. Berlin, Heidelberg: Springer; 2012; Lecture Notes in Computer Science 7578: 292-306.
[22] Tominaga S, Hirai K, Hoiriuchi T. Measurement and modeling of bidirectional characteristics of fluorescent objects. *Proceedings of the 16th International Symposium on Multispectral Colour Science*. New York: Springer-Verlag; 2014:35-42.
[23] Jung A, Hamika J, Marschner S, Dachsbacher C. A simple diffuse fluorescent BBRRDF model. *Proceedings of the Workshop on Material Appearance Modeling*; Geneva, Switzerland: The Eurographics Association; 2018:15-18.
[24] Jakob, W., *Mitsuba*; 2014; https://www.mitsuba-renderer.org/index_old.html.
[25] Veach E, Guibas L. Bidirectional estimators for light transport. *Photorealistic Rendering Techniques*. New York: Springer; 1995:145-167.
[26] Guarnera D, Guarnera GC, Ghosh A, Denk C, Glencross M. BRDF representation and acquisition. *Comput Graph Forum*. 2016;35(2):625-650.
[27] Kruse FA, Lefkoff AB, Boardman JB, et al. The spectral image processing system (SIPS)—interactive visualization and analysis of imaging spectrometer data. *Remote Sens Environ*. 1993; 44:145-163.

AUTHOR BIOGRAPHIES

Shoji Tominaga received a PhD in electrical engineering from Osaka University, Japan, in1975, joined Chiba University, Japan, where he was a professor (2006-2013), dean (2011-2013), a specially appointed researcher (2013-2018), and he is currently an adjunct professor at NTNU, Norway, and a visiting researcher at Nagano University, Japan. His research interests include fluorescent appearance analysis and synthesis, multispectral imaging, and material appearance. He is a life fellow IEEE, fellow IS&T, life fellow SPIE, fellow OSA, and honorary member of Color Science Association of Japan.

Giuseppe Claudio Guarnera received a PhD in computer science from the University of Catania, Italy in 2013. He is currently a lecturer in computer graphics and vision at the Department of Computer Science, University of York (UK) and a part-time Senior Researcher at NTNU. Since 2017 he is a Guest Researcher at Justus-Liebig University Giessen, Germany, Department of Psychology. His research interests include computer graphics, computer vision, and applications of visual perception in computer graphics.

How to cite this article: Tominaga S, Guarnera GC. Appearance synthesis of fluorescent objects with mutual illumination effects. *Color Res Appl*. 2021;1-15. doi:10.1002/col.22747